© 2014. Published by The Company of Biologists Ltd | Journal of Cell Science (2014) 127, 5007–5013 doi:10.1242/jcs.136457

SHORT REPORT

MAP1S controls microtubule stability throughout the cell cycle in human cells

Justus Tegha-Dunghu[1,*], Elena Bausch[1], Beate Neumann[2], Annelie Wuensche[3], Thomas Walter[3,‡], Jan Ellenberg[3] and Oliver J. Gruss[1,¶]

SUMMARY

Understanding the molecular basis for proper cell division requires a detailed functional analysis of microtubule (MT)-associated proteins. MT-associated protein 1S (MAP1S), the most ubiquitously expressed MAP1 family member, is required for accurate cell division. Here, using quantitative analysis of MT plus-end tracking, we show that MAP1S knockdown alters MT dynamics throughout the cell cycle. Surprisingly, MAP1S downregulation results in faster growing, yet short-lived, MTs in all cell cycle stages and in a global loss of MT acetylation. These aberrations correlate with severe defects in the final stages of cell division. In monopolar cytokinesis assays, we demonstrate that MAP1S guides MT-dependent initiation of cytokinesis. Our data underline the key role of MAP1S as a global regulator of MT stability and demonstrate a new primary function of MAP1S to regulate MT dynamics at the onset of cytokinesis.

KEY WORDS: Microtubule, Microtubule-associated protein, MAP1S, Microtubule dynamics, Cytokinesis

INTRODUCTION

Regulating dynamic microtubule (MT) functions involves post-translational tubulin modifications (Sirajuddin et al., 2014; for reviews, see Hammond et al., 2008; Perdiz et al., 2011; Janke and Bulinski, 2011; Magiera and Janke, 2014; Sirajuddin et al., 2014) and changes in the pattern of MT-associated proteins (MAPs) (for reviews, see Manning and Compton, 2008a; Manning and Compton, 2008b; Walczak and Heald, 2008). MAPs of the MAP1 family promote MT stability and modulate MT functions in mammalian cells. The MAP1 family comprises MAP1A, MAP1B and the most recently identified member, MAP1S (Dallol et al., 2007; Halpain and Dehmelt, 2006; Orban-Nemeth et al., 2005). MAP1S binds to MTs *in vitro* and colocalizes with MTs in cells (Dallol et al., 2007; Orban-Nemeth et al., 2005; Wong et al., 2004). In contrast to MAP1A and MAP1B, MAP1S is found not only in the nervous system, but also in liver, spleen, heart and other organs (Orban-Nemeth et al., 2005) where it seems to fulfil cell-type-specific functions (Eriksson et al., 2010; Eriksson et al., 2007; Xie et al., 2011a; Xie et al., 2011b). The more ubiquitous expression of MAP1S suggests that the protein sustains general MT-dependent functions. The knockdown of MAP1S in HeLa cells compromises spindle assembly, delays metaphase alignment and anaphase entry, and causes genome instability (Dallol et al., 2007). MAP1S was first identified in large-scale screens for spindle proteins (Sauer et al., 2005; Tegha-Dunghu et al., 2008), and has been shown to associate with the spindle in human and murine cells (Dallol et al., 2007; Orban-Nemeth et al., 2005). However, how MAP1S acts on MTs and how it influences the parameters of MT dynamics in different cell cycle stages remained unclear. Here, we show that MAP1S governs MT nucleation and MT dynamics in interphase and during early and late stages of M phase. We demonstrate that MAP1S-deficient cells assemble MTs faster, but that these MTs have a severely reduced lifetime in interphase, mitosis and during mitotic exit, when they are required to coordinate cytokinesis. Together with specific cytokinesis assays, our data underline that the primary function of MAP1S is to maintain balanced MT dynamics during mitosis as well as in cytokinesis.

RESULTS AND DISCUSSION

To analyze the role of MAP1S in MT organization in human cells, we tested different parameters that mark MT stability. MT stability correlates with acetylation of α-tubulin on lysine 40 (K40 acetylation) (Sirajuddin et al., 2014, for reviews, see Hammond et al., 2008; Perdiz et al., 2011; Janke and Bulinski, 2011; Magiera and Janke, 2014; Sirajuddin et al., 2014). We found that the amount of acetylated tubulin in cells where MAP1S was knocked down by small interfering RNA (siRNA) (Fig. 1A; Fig. 1B, left panel) was reduced by 60% (Fig. 1A; Fig. 1B, right panel). Quantitative indirect immunofluorescence in synchronized cells revealed a significant reduction in MT acetylation, on average by 58% in metaphase, 40% in anaphase, 68% in cytokinesis and 70% in interphase (S and G2) (Fig. 1C,D; see also supplementary material Fig. S3C). In contrast, MAP1S knockdown did not affect glutamylation of tubulin (supplementary material Fig. S1A). The levels of MAP1S itself remained constant during the cell cycle (supplementary material Fig. S1B), as was also indicated by the detection of MAP1S on MTs in mitosis and interphase (supplementary material Fig. S1C). Knockdown of Eml3, which also localizes to MTs in interphase and mitosis (Tegha-Dunghu et al., 2008), as well as the mitotic MT-binding protein TPX2 (Gruss et al., 2002), left MT acetylation unchanged (Fig. 1E; supplementary material Fig. S1D).

[1]Zentrum für Molekulare Biologie der Universität Heidelberg (ZMBH), DKFZ-ZMBH Alliance, Im Neuenheimer Feld 282, 69120 Heidelberg, Germany. [2]European Molecular Biology Laboratory (EMBL), Advanced Light Microscopy Facility Programme, Meyerhostr.1, 69117 Heidelberg, Germany. [3]European Molecular Biology Laboratory (EMBL), Cell Biology and Biophysics Programme, Meyerhostr.1, 69117 Heidelberg, Germany.
*Present address: Department of Biological Sciences, University of Alberta, Edmonton, Alberta T6G 2E9, Canada. ‡Present addresses: MINES ParisTech, PSL-Research University, CBIO-Centre for Computational Biology, 35 rue St Honoré 77300 Fontainebleau, France; Institut Curie, 75248 Paris CEDEX, France; and INSERM U900, 75248 Paris CEDEX, France

¶Author for correspondence (o.gruss@zmbh.uni-heidelberg.de)

Received 7 June 2013; Accepted 24 September 2014

Journal of Cell Science (2014) 127, 5007–5013 doi:10.1242/jcs.136457

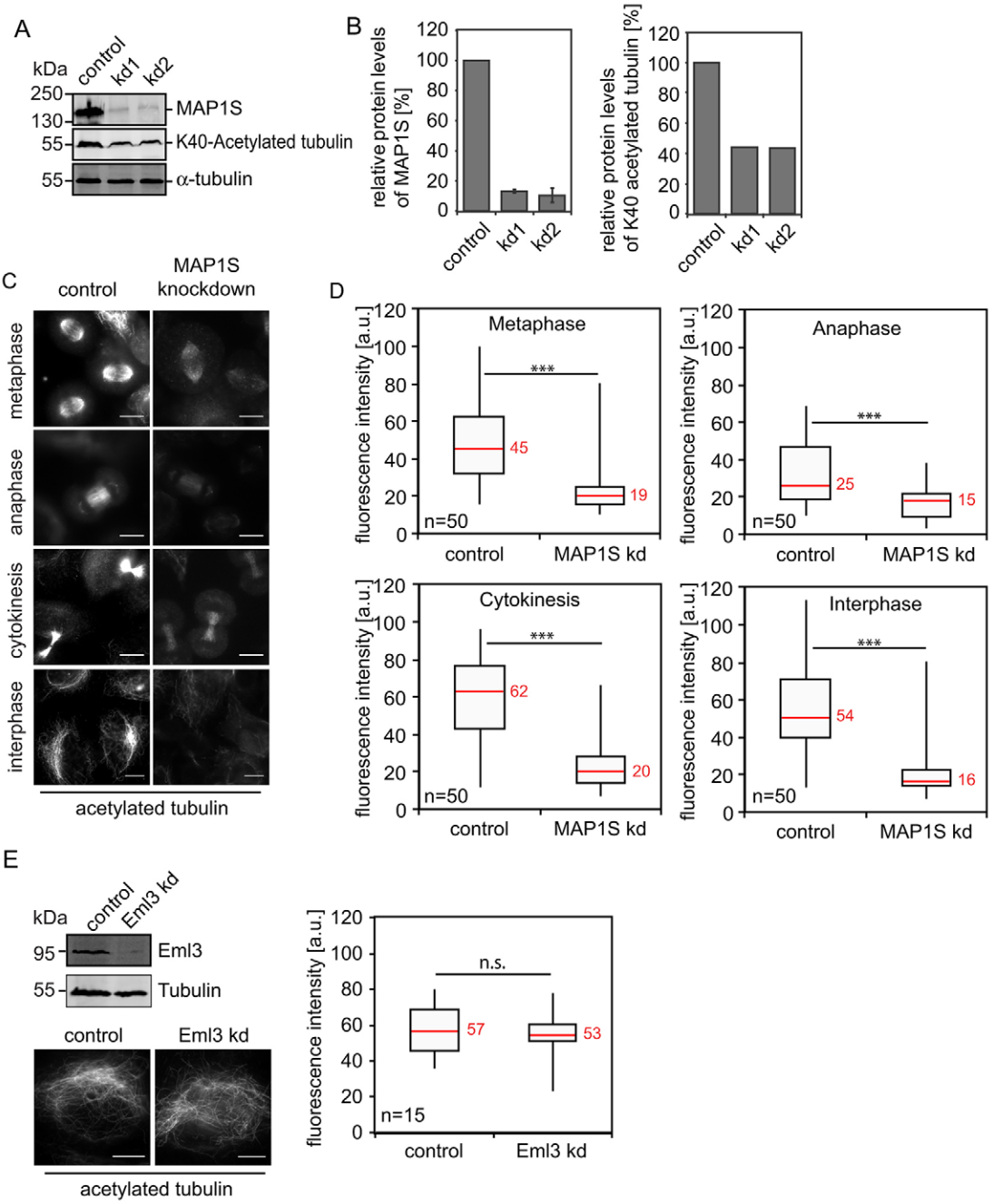

Fig. 1. K40-tubulin acetylation in MAP1S-knockdown cells. (A) Immunoblot and (B) quantification of the MAP1S knockdown efficiency (left panel, kd1 and kd2 represent knockdown with oligonucleotide 1 and 2, respectively) in HeLa cells, and relative changes in K40 α-tubulin acetylation (right panel) compared to the overall amount of α-tubulin. (C) K40 α-tubulin acetylation as analyzed by immunofluorescence after MAP1S knockdown (kd1) in synchronized cells at the indicated stages of the cell cycle. (D) Quantification of individual cells (n=50) as shown in C. (E) K40 α-tubulin acetylation after knockdown of the MAP Eml3. Upper panel: immunoblot to detect Eml3 compared to α-tubulin; lower panel: K40 α-tubulin acetylation after Eml3 knockdown in single cells; right panel: quantification of the K40 α-tubulin acetylation upon Eml3 knockdown, n=15 cells. ***P<0.001; n.s., non-significant (unpaired two-tailed Student's t-test). MW, position of molecular mass markers. Scale bars: 10 μm.

To evaluate a general function of MAP1S in the control of MT stability, we performed MT regrowth assays in interphase and mitotic cells after cold-induced MT depolymerization (Fig. 2), and directly measured MT dynamics in intact cells (Fig. 3). Although MTs regrew quickly (2–5 min) in control cells, only inefficient MT repolymerization was seen in MAP1S-knockdown cells, as determined by monitoring end-binding protein 3 (EB3, also known as MAPRE3) as a plus-end marker (Fig. 2). To confirm the specificity of our observation, we expressed a siRNA-resistant version of MAP1S fused to mCherry. mCherry–MAP1S localized to MTs in interphase and mitosis (supplementary material Fig. S2A) and escaped the knockdown, unlike endogenous MAP1S (supplementary material Fig. S2B). We then quantified MT regrowth on the basis of the EB3 signal using a previously established algorithm for the quantification of aster size (Yokoyama et al., 2008). Knockdown of MAP1S (supplementary

Journal of Cell Science (2014) 127, 5007–5013 doi:10.1242/jcs.136457

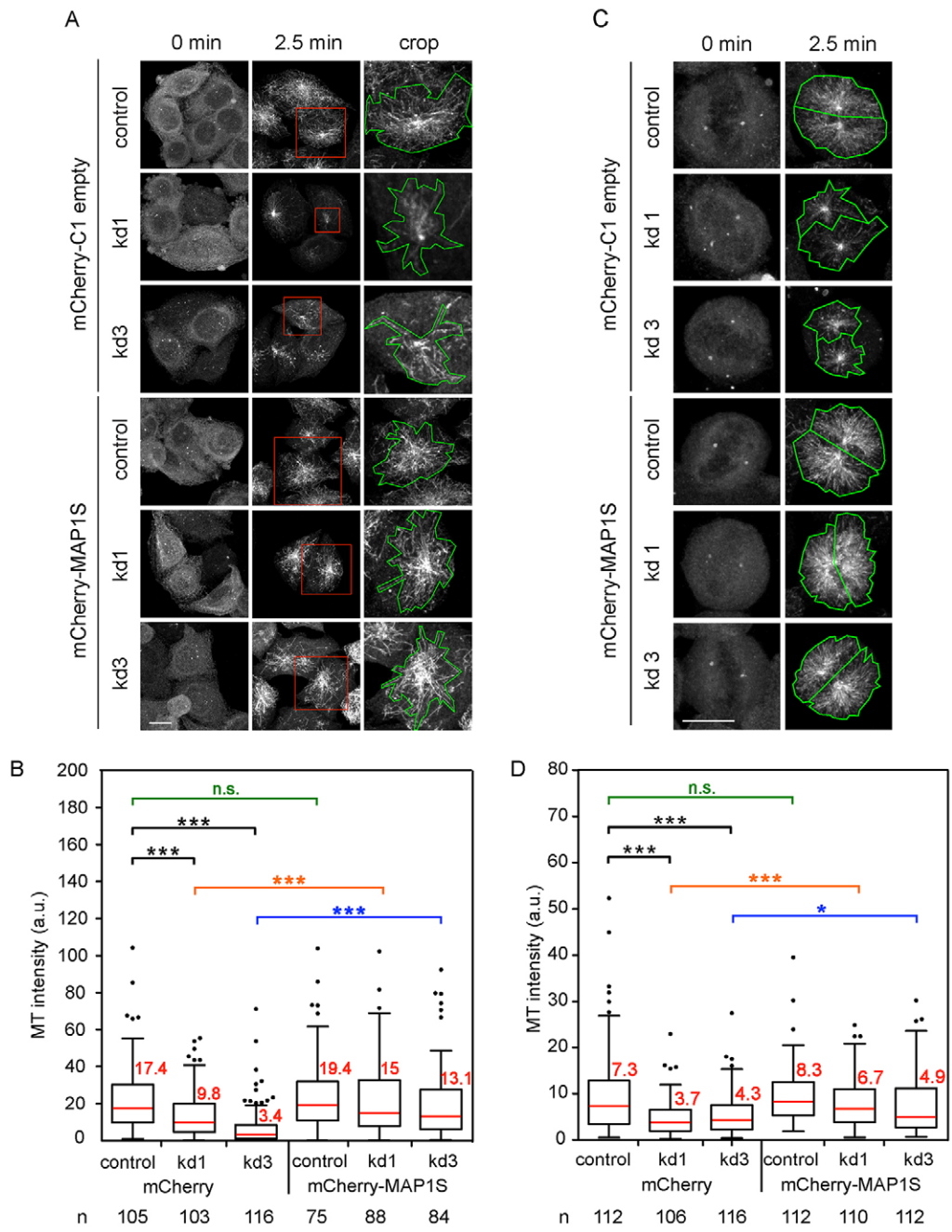

Fig. 2. MAP1S is rate limiting for MT regrowth. MT regrowth for 2.5 min after cold-induced depolymerization. EGFP–EB3-expressing HeLa cells were analyzed after control knockdown, MAP1S knockdown (kd2 and kd3 represent knockdown with oligonucleotide 2 and 3, respectively), or in control or knockdown cells transiently expressing siRNA-resistant mCherry–MAP1S. (A,C) EB3 detection in single cells in interphase (A) or mitosis (C) after MT regrowth; red squares in A indicate magnified cells used for quantification in B. Green lines (A and C) indicate quantified areas. Scale bars: 10 µm. (B,D) Quantification of MT regrowth as visualized in A and C; total fluorescence of regrowing MT asters from three independent experiments was quantified and plotted in box plots. The box shows the interquartile range (IQR), median values are shown in red and the whiskers represent 1.5 x IQR minus/plus the 25th/75th percentile. Possible outliers are shown as individual dots. *n*=number of aster structures. **P*<0.05; ****P*<0.001; n.s., not significant (unpaired two-tailed Student's *t*-test).

material Fig. S3C) significantly reduced the size of the re-growing asters in interphase (Fig. 2A,B) and mitosis (Fig. 2C,D), but aster sizes could be restored upon mCherry–MAP1S expression in both cell cycle phases (Fig. 2A–D). These data indicate that MAP1S is rate limiting for efficient MT polymerization in interphase and mitosis. Moreover, the rescue experiments clearly confirm the specificity of our knockdown conditions.

To quantitatively reveal key characteristics of MT dynamics after MAP1S knockdown (supplementary material Fig. S3C), we imaged cells expressing EB3–GFP for 60 s and performed automated image analysis of MT plus-ends (Matov et al., 2010; Sironi et al., 2011). In mitotic cells (Fig. 3A), the characteristic lifetime of individual EB3 comets was reduced upon MAP1S knockdown, but growth speed (average velocity) was increased by up to 40%. The average length of growing MTs also increased significantly whereas the average number of tracks remained unaffected (Fig. 3B). MAP1S knockdown in interphase cells yielded MTs with shorter half-lives but higher growth speeds (Fig. 3E), resulting in comparable characteristic track length values. MAP1S knockdown with siRNA oligonucleotide 1 and 2 in interphase significantly reduced the number of plus-end tracks per cell, by 40% and 45%, respectively (Fig. 3E). Reduced numbers of growing MTs were readily apparent in individual cells (see magnifications of single frames in Fig. 3D, and projections in Fig. 3C), and the overall track number was lower than in any control cell measured in 44% and 24% of MAP1S-knockdown cells (with siRNA oligonucleotide 1 and 2, respectively; supplementary material Fig. S3A). We found a similar MT architecture in control and MAP1S-knockdown cells despite fewer growing MTs upon MAP1S knockdown (supplementary material Fig. S3B,C).

Journal of Cell Science (2014) 127, 5007–5013 doi:10.1242/jcs.136457

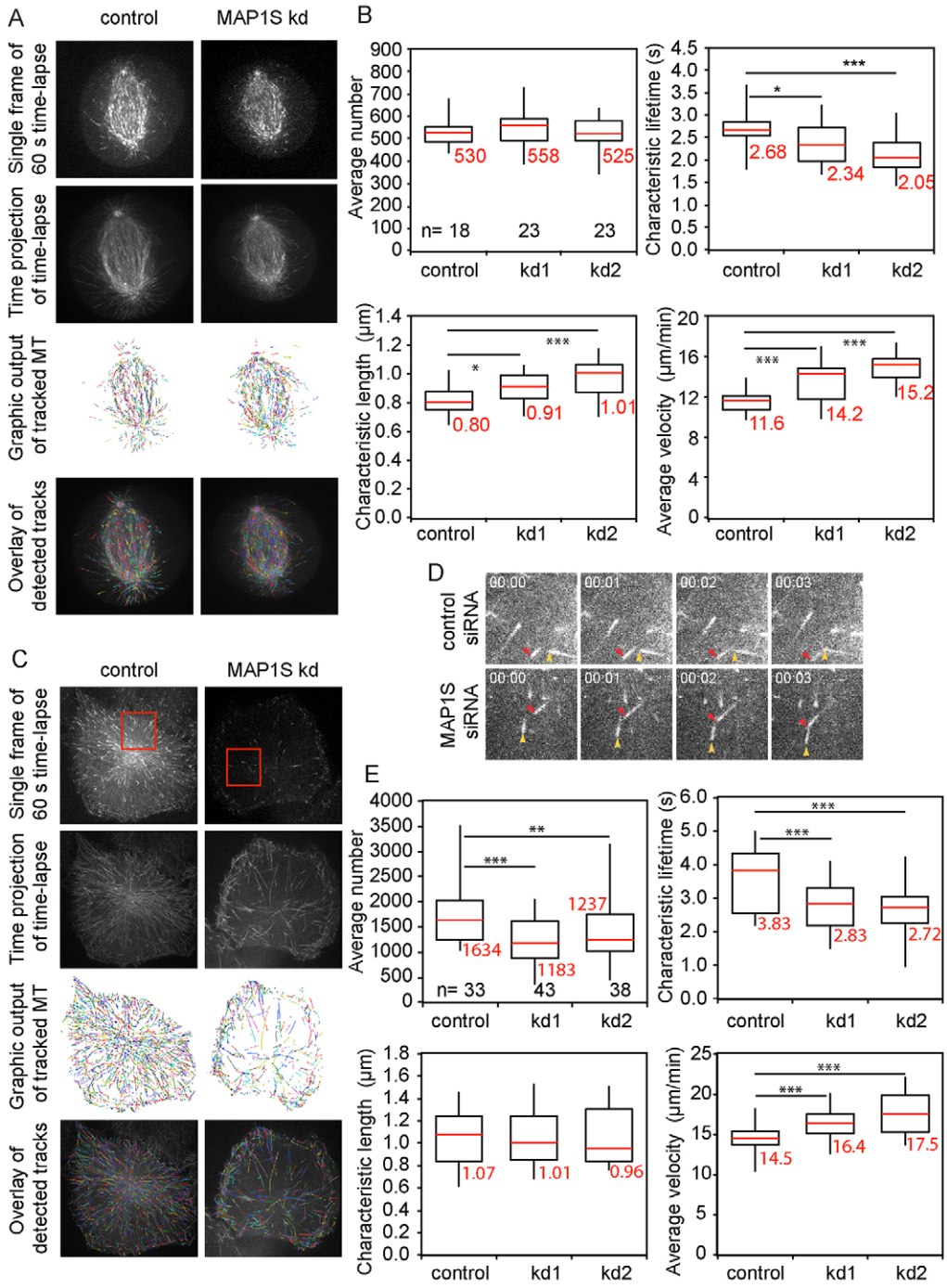

Fig. 3. Time-lapse recordings of EB3–EGFP in HeLa cells after knockdown of MAP1S. (A,C) EGFP–EB3 tracking in single (A) mitotic and (C) interphase cells. Examples of single timeframes (top), time projections from 60-s recordings at 400 ms intervals (second row), pseudocolor representation of tracks that were automatically detected (third row), and overlay of time projection and pseudocolor representation of tracks (bottom) after knockdown of MAP1S (with oligonucleotide 1). (B,E) Quantification of average (median) track number, characteristic track lifetime, characteristic track length and average (median) track velocity, as indicated and described previously (Sironi et al., 2011), after knockdown (kd1 and kd2 represent knockdown with oligonucleotide 1 and 2, respectively) of MAP1S for (B) mitotic cells and (E) interphase cells. The box represents the interquartile range; the median values are shown in red, and the whiskers represent the range. *n*=cell number; measurements were from three independent experiments; please note that several hundred tracks were measured on average in each cell. $^{**}P<0.01$; $^{***}P<0.001$ (unpaired two-tailed Student's *t*-test). (D) Single frames (see red squares in C) of EGFP–EB3, to show consecutive time lapses (400 ms). Yellow and red arrowheads indicate moving EGFP–EB3 tracks.

Our above results indicate that the MT dynamics is altered in mitosis, but that the reduction in MT stability is even more pronounced in interphase. At the transition from mitosis to interphase, spindle MTs coordinate assembly of the contractile ring. The high density of MTs in the central spindle precludes direct measurements of MT dynamics at this point. In a sensitive assay for MT function in cytokinesis, however, cells can be arrested in mitosis with a single symmetric, monopolar array of MTs with free plus ends. When CDK1 is inhibited, these cells are forced to exit mitosis. MTs form a focused bundle, polarize the cortex and mediate accumulation of contractile ring effectors, such as Aurora B, at a single position, where cytokinesis occurs (monopolar cytokinesis) (Hu et al., 2008). We used such an assay and found that MT plus-end tracking in cells assembling monopolar MT structures was readily possible (Fig. 4A,B; supplementary material Fig. S3C). We observed a significant increase in the average velocity of tracks and a significant reduction in characteristic track lifetimes, which resulted in a reduced characteristic track length (Fig. 4B). Importantly, as in interphase, the overall track number decreased after MAP1S knockdown (Fig. 4B). This suggests that the stabilization of MTs during cytokinesis relies on MAP1S. In order to determine the functional consequences of MAP1S knockdown for monopolar cytokinesis, we correlated the timing of Aurora B polarization with the time after CDK1 inhibition (Fig. 4C,D). Knockdown of MAP1S still allowed polarization and accumulation of Aurora B

Journal of Cell Science (2014) 127, 5007–5013 doi:10.1242/jcs.136457

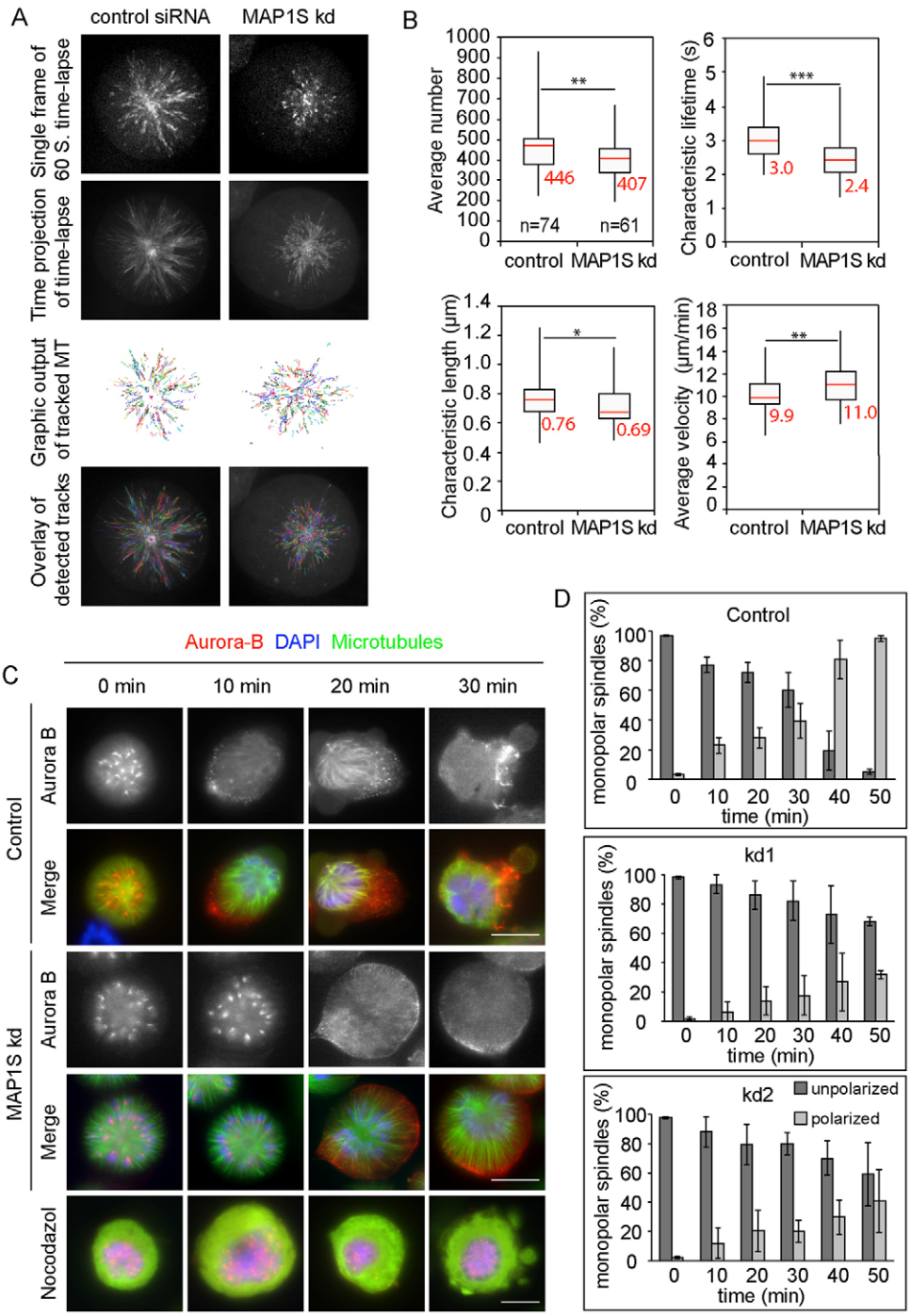

Fig. 4. Analyzing the function of MAP1S in cell division using monopolar cytokinesis assays. (A) EGFP–EB3 tracking in cells during monopolar cytokinesis. Examples of single timeframes (top), time projections from 60-s recordings at 400 ms intervals (second row), pseudocolor representation of tracks that were automatically detected (third row), and overlay of time projection and pseudocolor representation of tracks (bottom) after knockdown of MAP1S (with oligonucleotide 1). (B) Quantification of average (median) track number, average track lifetime, average track length and average track velocity, as indicated and described previously (Sironi et al., 2011), after knockdown of MAP1S (with oligonucleotide 1). The box represents the interquartile range; the median values are shown in red, and the whiskers represent the range. *n*=cell number; measurements were from three independent experiments; please note that several 100 tracks were measured on average in each cell. **P*<0.05; ***P*<0.01; ****P*<0.001 (unpaired two-tailed Student's *t*-test). (C) Immunofluorescence detecting Aurora B (red), tubulin (green) and DAPI (blue). Scale bars: 10 µm. (D) The relative number of cells showing a polarized Aurora B signal (as shown in C) was determined at the time points indicated. At least 1000 cells were counted in total in three independent experiments. The quantification shows mean±s.e.m. from the three independent experiments. kd1 and kd2 represent knockdown with oligonucleotide 1 and 2, respectively.

yet with significant delay: MAP1S knockdown changed the efficiency of polarization at all time points tested (Fig. 4C,D) confirming the key role of MAP1S as a regulator of proper MT dynamics at the onset of cytokinesis.

It has been published previously that MAP1S knockdown leads to defects in spindle formation and mitotic progression resulting in chromosome segregation errors (Dallol et al., 2007; Neumann et al., 2010; see http://www.mitocheck.org). Mitotic defects have been correlated with defects in centrosomal nucleation and spindle MT production suggesting a function of MAP1S at the centrosome in particular, and on mitotic MTs in general (Dallol et al., 2007). Here, we show that MT regrowth is delayed upon knockdown of MAP1S in interphase and mitosis, indicating that loss of MAP1S retards nucleation and/or proper polymerization of new MTs. MAP1S seems to act in at least two ways. First, it supports nucleation or an early growth phase of MTs. This is obvious in interphase and cytokinesis, when the number of MT tracks is reduced after downregulation of MAP1S. In contrast, possibly owing to the general increase in MT nucleation, MAP1S seems not to be rate limiting for nucleation in mitosis. Second, MAP1S controls the growth speed and half life of MTs at all stages of the cell cycle. Its knockdown leads to faster growing MTs at the expense of shorter phases of growth. Interestingly, the respective impact of MAP1S on these two main parameters

(polymerization velocity and MT half life) varies during the cell cycle. A strong increase in polymerization speed results in longer tracks despite a reduced life-time during mitosis. In contrast, shorter life-times and increased growth speed cancel each other out during interphase, resulting in unchanged MT length. Importantly, shorter MT tracks arise in cytokinesis, when downregulation of MAP1S affects life-time more dramatically than growth speed. This indicates that, when these cells enter cytokinesis, they face the problem of producing fewer, and faster growing, less-stable MTs. This will compromise delivery of cytokinetic effectors, delay polarization in monopolar cytokinesis and, in regular cytokinesis, compromise proper positioning of the cytokinetic machinery with respect to spindle MTs. Indeed, the polarization of the monopolar MT arrays in MAP1S-knockdown cells is significantly delayed, indicating slower progression through cytokinesis. Our data consistently underline a new, hitherto unknown, function of MAP1S in cytokinesis. MAP1S stabilizes MTs at the transition from M phase to interphase (i.e. in cytokinesis) when MT dynamics turn back from the highly dynamic mitotic status to parameters that promote the stable array of interphase MT.

MATERIALS AND METHODS

Antibodies and immunoblotting

Primary antibodies for immunoblotting and immunofluorescence were: mouse anti-α-tubulin (T9026, Sigma), mouse anti-K40 acetylated α-tubulin (Santa Cruz Biotechnology, sc-23950), mouse anti-glutamylated tubulin (GT335, AdipoGen, Liestal, Switzerland), mouse anti-MAP1S (anti C19orf5, AG10006, A&G Pharmaceuticals, Inc., Columbia, MD), rabbit anti-Aurora B (Abcam, ab2254); rabbit anti-TPX2 (Gruss et al., 2002) and guinea pig anti-Eml3 (Tegha-Dunghu et al., 2008) antibodies. Immunoblots were analyzed using Odyssey Infrared LICOR imager (Li-COR Biosciences GmbH).

Cell culture, cell lines and reagents

HeLa cells were cultured in Dulbecco's modified Eagle's medium (DMEM) with 10% fetal calf serum (FCS), 2 mM glutamine and penicillin-streptomycin (Life Technologies) at 37℃ and under 5% CO_2. We initiated monopolar cytokinesis using the Eg5 (also known as KIF11) inhibitor S-trityl-L-cysteine (STLC) for 5 h to arrest cells in mitosis followed by incubation with 3 µM of the CDK1 inhibitor RO-3306 or Purvalanol A (both Merck/Calbiochem) at 2 µM. To synchronize cells in S phase, we used 2 mM thymidine (Sigma) for 19 h followed by 9 h release and another 16 h in thymidine. After the second block, cells were released and samples taken every hour for 15 h. To depolymerize MTs, cells were treated for 60 min on ice and incubated at 37℃ to allow MT regrowth. All experimental conditions are summarized in supplementary material Fig. S3C.

Immunofluorescence and microscopy

HeLa cells seeded on coverslips were fixed either in 3% paraformaldehyde for 10 min at room temperature, or in methanol at −20℃ for 3 min. Images were taken with the Olympus CellR-PointFRAP IX81 using a PLAPO 100×/1.45 NA oil-immersion objective, or on a Leica LSM780 confocal imaging system using a PLAN APOCHROMAT 63×/1.4 NA oil-immersion objective, and processed in Photoshop CS5 software or ImageJ64 1.45S.

Expression constructs, transfection and siRNA

PCR-amplified cDNAs (Imagenes/SourceBio) were ligated into monomeric EYFP-C3 or EGFP-C1 plasmids (Clontech). For transfection of cDNAs we used Lipofectamine 2000 and for siRNAs, Lipofectamine RNAiMax (both Life Technologies). siRNA duplexes targeting MAP1S, s30423 (silencer select, oligonucleotide 1), HSS124109 (Stealth, oligonucleotide 2) and s30423 (silencer select, oligonucleotide 3), were obtained from Life Technologies. Oligonucleotide 1 alone was used for experiments in Fig. 1C,D and Fig. 4A,B. Oligonucleotides 1 and 2 were used in all figures labeled as kd1 and kd2. Oligonucleotides 1 and 3 were used in Fig. 2 (kd1 and kd3). To knockdown Eml3 (Tegha-Dunghu et al., 2008), siRNA HSS137986 (Stealth, Life technologies) was used. The siRNA-resistant MAP1S cDNA was synthesized (Gene Arts/Life technologies) with three silent mutations in the sequence bound by the seed region of siRNAs and ligated into the pmCherry-C1 expression vector (Clontech).

Live-cell imaging of MT plus-ends in intact cells

HeLa EGFP–EB3-expressing cells (Sironi et al., 2011) were seeded into ibidi chambers (ibidi GmbH, Germany). Imaging was performed on a PerkinElmer UltraView Spinning Disc with a 100×/1.4 NA oil-immersion objective and a Hamamatsu orca-R^2 camera in 37℃ microscope incubators using medium without Phenol Red (Life technologies). Time-lapse images were acquired with a 300-ms exposure at a temporal resolution of 400 ms for 60 s. Cropping of single frames was performed with in ImageJ using a Gaussian blur filter of radius 2 and analyzed with a multiple particle tracking software (Sironi et al., 2011).

Tracking of MTs in interphase and quantitative analysis of MT dynamics

After processing raw data with ImageJ, we used a MATLAB-based program to detect and track the tips of polymerizing MTs. Tracking algorithms are as described previously (Sironi et al., 2011).

Quantification of MT regrowth

Z-stacks of the EB3–EGFP signal from HeLa cells stably expressing the protein were taken on a Zeiss LSM 780 confocal microscope. After *Z*-projection and background subtraction, the sum intensity of the EB3 signal was measured within single cells. For the measurement, we used a previously developed MATLAB macro (Yokoyama et al., 2008) after manually defining the regrowth area.

Statistical data analysis

For experiments in Fig. 1D,E, Fig. 2B,D, Fig. 3B,E as well as Fig. 4B we displayed the data sets in box plots showing median values (red), upper and lower quartiles, and minimum and maximum values. In Fig. 4D, bars with mean±s.e.m. summarize the quantification. Significance values in Fig. 1D,E, Fig. 2B,D, Fig. 3B,E and Fig. 4B,D were calculated by Student's *t*-tests (two-tailed). *P*-values for all tests were defined as follows: $*P<0.05$, $**P<0.01$, $***P<0.001$, $****$ $P<0.0001$.

Acknowledgements

We thank Elmar Schiebel (ZMBH, Heidelberg, Germany) for critically reading the manuscript and Thomas Mayer (University of Konstanz, Germany) for discussions.

Competing interests

The authors declare no competing interests.

Author contributions

J.T.D. did the experiments on MT acetylation, the initial regrowth assay, MT dynamics measurements and the cytokinesis assay. E.B. performed rescue experiments and the quantification of MT regrowth. B.N., A.W. and T.W. performed time-lapse experiments and helped with the quantification of MT dynamics measurements. J.E. contributed to experiment design and manuscript writing. O.J.G. initially analyzed MT regrowth by confocal microscopy, designed experiments and wrote the manuscript.

Funding

The work was supported by a start-professorship funded by the German excellence initiative [grant number ZUK 49/2 8.1.007 to O.J.G.]. J.T.D. was supported by the DKFZ-ZMBH-Alliance. E.B. was a member of HBIGS graduate school.

Supplementary material

Supplementary material available online at
http://jcs.biologists.org/lookup/suppl/doi:10.1242/jcs.136457/-/DC1

References

Dallol, A., Cooper, W. N., Al-Mulla, F., Agathanggelou, A., Maher, E. R. and Latif, F. (2007). Depletion of the Ras association domain family 1, isoform A-associated novel microtubule-associated protein, C19ORF5/MAP1S, causes mitotic abnormalities. *Cancer Res.* **67**, 492-500.

Eriksson, M., Samuelsson, H., Samuelsson, E. B., Liu, L., McKeehan, W. L., Benedikz, E. and Sundström, E. (2007). The NMDAR subunit NR3A interacts with microtubule-associated protein 1S in the brain. *Biochem. Biophys. Res. Commun.* **361**, 127-132.

Eriksson, M., Samuelsson, H., Björklund, S., Tortosa, E., Avila, J., Samuelsson, E. B., Benedikz, E. and Sundström, E. (2010). MAP1B binds to the NMDA receptor subunit NR3A and affects NR3A protein concentrations. *Neurosci. Lett.* **475**, 33-37.

Gruss, O. J., Wittmann, M., Yokoyama, H., Pepperkok, R., Kufer, T., Silljé, H., Karsenti, E., Mattaj, I. W. and Vernos, I. (2002). Chromosome-induced microtubule assembly mediated by TPX2 is required for spindle formation in HeLa cells. *Nat. Cell Biol.* **4**, 871-879.

Halpain, S. and Dehmelt, L. (2006). The MAP1 family of microtubule-associated proteins. *Genome Biol.* **7**, 224.

Hammond, J. W., Cai, D. and Verhey, K. J. (2008). Tubulin modifications and their cellular functions. *Curr. Opin. Cell Biol.* **20**, 71-76.

Hu, C. K., Coughlin, M., Field, C. M. and Mitchison, T. J. (2008). Cell polarization during monopolar cytokinesis. *J. Cell Biol.* **181**, 195-202.

Janke, C. and Bulinski, J. C. (2011). Post-translational regulation of the microtubule cytoskeleton: mechanisms and functions. *Nat. Rev. Mol. Cell Biol.* **12**, 773-786.

Magiera, M. M. and Janke, C. (2014). Post-translational modifications of tubulin. *Curr. Biol.* **24**, R351-R354.

Manning, A. L. and Compton, D. A. (2008a). SnapShot: Nonmotor proteins in spindle assembly. *Cell* **134**, 694.

Manning, A. L. and Compton, D. A. (2008b). Structural and regulatory roles of nonmotor spindle proteins. *Curr. Opin. Cell Biol.* **20**, 101-106.

Matov, A., Applegate, K., Kumar, P., Thoma, C., Krek, W., Danuser, G. and Wittmann, T. (2010). Analysis of microtubule dynamic instability using a plus-end growth marker. *Nat. Methods* **7**, 761-768.

Neumann, B., Walter, T., Hériché, J. K., Bulkescher, J., Erfle, H., Conrad, C., Rogers, P., Poser, I., Held, M., Liebel, U. et al. (2010). Phenotypic profiling of the human genome by time-lapse microscopy reveals cell division genes. *Nature* **464**, 721-727.

Orbán-Németh, Z., Simader, H., Badurek, S., Tranciková, A. and Propst, F. (2005). Microtubule-associated protein 1S, a short and ubiquitously expressed member of the microtubule-associated protein 1 family. *J. Biol. Chem.* **280**, 2257-2265.

Perdiz, D., Mackeh, R., Poüs, C. and Baillet, A. (2011). The ins and outs of tubulin acetylation: more than just a post-translational modification? *Cell. Signal.* **23**, 763-771.

Sauer, G., Körner, R., Hanisch, A., Ries, A., Nigg, E. A. and Silljé, H. H. (2005). Proteome analysis of the human mitotic spindle. *Mol. Cell. Proteomics* **4**, 35-43.

Sirajuddin, M., Rice, L. M. and Vale, R. D. (2014). Regulation of microtubule motors by tubulin isotypes and post-translational modifications. *Nat. Cell Biol.* **16**, 335-344.

Sironi, L., Solon, J., Conrad, C., Mayer, T. U., Brunner, D. and Ellenberg, J. (2011). Automatic quantification of microtubule dynamics enables RNAi-screening of new mitotic spindle regulators. *Cytoskeleton (Hoboken)* **68**, 266-278.

Tegha-Dunghu, J., Neumann, B., Reber, S., Krause, R., Erfle, H., Walter, T., Held, M., Rogers, P., Hupfeld, K., Ruppert, T. et al. (2008). EML3 is a nuclear microtubule-binding protein required for the correct alignment of chromosomes in metaphase. *J. Cell Sci.* **121**, 1718-1726.

Walczak, C. E. and Heald, R. (2008). Mechanisms of mitotic spindle assembly and function. *Int. Rev. Cytol.* **265**, 111-158.

Wong, E. Y., Tse, J. Y., Yao, K. M., Lui, V. C., Tam, P. C. and Yeung, W. S. (2004). Identification and characterization of human VCY2-interacting protein: VCY2IP-1, a microtubule-associated protein-like protein. *Biol. Reprod.* **70**, 775-784.

Xie, R., Nguyen, S., McKeehan, K., Wang, F., McKeehan, W. L. and Liu, L. (2011a). Microtubule-associated protein 1S (MAP1S) bridges autophagic components with microtubules and mitochondria to affect autophagosomal biogenesis and degradation. *J. Biol. Chem.* **286**, 10367-10377.

Xie, R., Wang, F., McKeehan, W. L. and Liu, L. (2011b). Autophagy enhanced by microtubule- and mitochondrion-associated MAP1S suppresses genome instability and hepatocarcinogenesis. *Cancer Res.* **71**, 7537-7546.

Yokoyama, H., Gruss, O. J., Rybina, S., Caudron, M., Schelder, M., Wilm, M., Mattaj, I. W. and Karsenti, E. (2008). Cdk11 is a RanGTP-dependent microtubule stabilization factor that regulates spindle assembly rate. *J. Cell Biol.* **180**, 867-875.